Mesoscopic quantum transport: Resonant tunneling in the presence of a strong Coulomb interaction

Herbert Schoeller* and Gerd Schön
Institut für Theoretische Festkörperphysik, Universität Karlsruhe, 76128 Karlsruhe, Germany
(Received 22 July 1994)

Coulomb-blockade phenomena and quantum fluctuations are studied in mesoscopic metallic tunnel junctions with high charging energies. If the resistance of the barriers is large compared to the quantum resistance, transport can be described by sequential tunneling. Here we study the influence of quantum fluctuations. They are strong when the resistance is small or the temperature is very low. A real-time approach is developed that allows the diagrammatic classification of resonant tunneling processes where different electrons tunnel coherently back and forth between the leads and the metallic island. With the help of a nonperturbative resummation technique we evaluate the spectral density, which describes the charge excitations of the system. From it, physical quantities of interest such as current and average charge can be deduced. Our main conclusions are as follows: An energy renormalization leads to a logarithmic temperature dependence of the renormalized system parameters. A finite lifetime broadening can change the classical picture drastically. It gives rise to a strong flattening of the Coulomb oscillations for low resistances, but in the Coulomb-blockade regime inelastic electron cotunneling persists. The effects become important at temperatures that are accessible in experiments.

I. INTRODUCTION

Quantum transport through mesoscopic metallic islands coupled to large reservoirs has been the subject of many theoretical and experimental investigations in recent years.[1–3] The small size of these systems implies a very strong Coulomb interaction which gives rise to a variety of single-electron phenomena. When the temperature T is low compared to the charging energy E_C, tunneling can be suppressed by the Coulomb blockade. However, when the energy difference Δ_0 between two adjacent charge states is comparable to the temperature or the bias voltage, a current can flow through the system. As a consequence, the differential conductance shows a peak structure as function of an external gate voltage V_g (linear response) or the bias voltage V (nonlinear response). In the absence of a dissipative environment, the smearing of these oscillations is dominated by the temperature provided that the resistance R_T of a single barrier is much higher than the quantum resistance $R_K = \frac{h}{e^2}$, i.e., $\alpha_0 \equiv \frac{1}{4\pi^2}\frac{R_K}{R_T} \ll 1$. In this classical regime, transport through the system is achieved by sequences of uncorrelated tunneling processes which can be described by lowest-order perturbation theory in the coupling between the leads and the metallic island. The corresponding classical rates can be used to set up a master equation[4–8] from which the charge probabilities and the current can be calculated. However, for very low temperatures or when the coupling α_0 becomes larger, quantum fluctuations set on[9–15] and the classical picture breaks down for two reasons. First, the resummation of the leading logarithmic terms in $\alpha_0 \ln(\frac{E_C}{2\pi T})$ leads to a renormalization of the gap Δ_0 and the dimensionless conductance α_0,

$$\tilde{\Delta}_0 = \frac{\Delta_0}{1 + 2\alpha_0 \ln\left(\frac{E_C}{2\pi T}\right)}, \quad \tilde{\alpha}_0 = \frac{\alpha_0}{1 + 2\alpha_0 \ln\left(\frac{E_C}{2\pi T}\right)}, \quad (1)$$

provided that $\tilde{\Delta}_0 \leq T$. Throughout this work, we set $\hbar = k = 1$ and consider only the case of a wide junction with many transverse channels. This renormalization is only important if $T \leq \frac{E_C}{2\pi} \exp[-1/(2\alpha_0)]$, which is an experimentally relevant temperature if α_0 is not too small. Secondly, the consideration of coherent processes where the electrons can tunnel an arbitrary number of times between the leads and the island (resonant tunneling) gives rise to an energy and temperature dependent broadening of the charge states. Thus, one cannot only overcome the Coulomb blockade by thermal broadening but also by quantum fluctuations due to higher-order processes. For $\tilde{\Delta}_0 \gg T$, this phenomenon is known as inelastic cotunneling[16,17] and can be obtained by a systematic analysis to second-order perturbation theory in α_0. Important results of the present work are that resonant tunneling processes describe the crossover from cotunneling to sequential tunneling and can also give rise to important corrections to the classical result in the regime $\tilde{\Delta}_0 \leq T$, where the conductance reaches its maximum value. Furthermore, we will show that they are especially important when $\pi\tilde{\alpha}_0 \sim 1$, which for finite temperatures can be realized for a sufficiently large value for α_0. Thus, by lowering the height of the tunneling barriers we expect that effects due to energy renormalization and finite lifetimes are observable in a real experiment at realistic temperatures. The observation of pure energy renormalization effects without the influence of fi-

nite lifetime broadening is difficult since $2\alpha_0 \ln(\frac{E_C}{2\pi T}) \sim 1$ together with $\pi\tilde{\alpha}_0 \ll 1$ is only possible for very low temperatures.

Charge fluctuations in the equilibrium case (single-electron box) have been studied before by many authors. In Ref. 13, a systematic perturbation expansion has been performed up to second order in α_0 including all possible charge states. This is a good approximation whenever the parameter $2\alpha_0 \ln(\frac{E_C}{2\pi T})$ (and, consequently, also $\pi\tilde{\alpha}_0$) is small compared to unity, i.e., the energy renormalization and the finite broadening are accounted for in a perturbative way. In Refs. 11, 12, and 14 the leading logarithmic terms together with certain improvements for larger values of α_0 (Ref. 14) have been considered in the two charge state approximation. Since finite broadening effects are neglected, these approaches are valid in the low temperature regime, where $\pi\tilde{\alpha}_0 \ll 1$ and lead to the same renormalization effects as given by Eq. (1). In the nonequilibrium case (SET transistor), the crossover from sequential tunneling to inelastic cotunneling has been studied in (Refs. 18–21) by introducing a finite and constant lifetime into the expression of electron cotunneling. The results agree with experiments[22,23] in the parameter regime $2\alpha_0 \ln(\frac{E_C}{2\pi T}) \ll 1$ and $\pi\tilde{\alpha}_0 \ll 1$, where renormalization effects and the energy dependence of the finite lifetime can be neglected.

In the present work, we will develop a systematic diagrammatic technique in real time to identify the processes of sequential tunneling, inelastic cotunneling, and resonant tunneling. Using the two charge state approximation, we can resum the corresponding diagrams analytically and obtain closed expressions for the density matrix and all Green's functions. The spectral density describing the charge excitations of the system is shown to contain an energy renormalization as well as a finite broadening. Both are retained which is crucial to obtain a conserving theory which obeys sum rules and current conservation. The basic starting point of our technique, the real-time representation of the density matrix, is closely related to path integral representations formulated in connection with dissipation[24,25] or tunneling in metallic junctions.[5,26] It is a well-suited method to perform a nonperturbative analysis in the coupling to the reservoirs while taking into account exactly the strong correlations due to the Coulomb interaction. Thus, usual Green's function techniques, either for equilibrium[27,28] or nonequilibrium[29,30] systems, cannot be used here. The same problem arises in the context of local strongly correlated Fermi systems like, e.g., the Kondo or Anderson model.[31,32] For these systems very similiar diagrammatic techniques to our ones have been used by Barnes[33] for the equilibrium case starting from a slave-boson description. Another example is a work by Rammer,[34] who developed the same graphical language within a density-matrix description of the dynamics of a particle coupled to a heat bath. Finally, the whole technique presented in this work can also be formulated very elegantly in terms of Liouville operators using projection operator techniques developed by Loss and Schoeller in Ref. 35. These relationships as well as the generalization to other systems like, e.g., quantum dots with arbitrary many-particle correlations or time-dependent Hamiltonians will be the subject of forthcoming works.

II. HAMILTONIAN AND PHYSICAL QUANTITIES

A small metallic island coupled via high tunneling barriers to two leads and capacitatively to an external gate voltage (SET transistor, see Fig. 1) is described by the following Hamiltonian

$$H = H_L + H_R + H_I + V + H_T = H_0 + H_T. \tag{2}$$

Here,

$$H_r = \sum_{kn} \epsilon^r_{kn} a^\dagger_{krn} a_{krn}, \qquad H_I = \sum_{ln} \epsilon_{ln} c^\dagger_{ln} c_{ln} \tag{3}$$

describe the noninteracting electrons in the two leads $r = L, R$ and on the island where n is the transverse channel index which includes the spin. The wave vectors k and l numerate the states of the electrons for fixed r and n (a subindex k_{rn} or l_n has been omitted for simplicity). The Coulomb interaction V obtained by straightforward electrostatic considerations[1,4,10] is given by

$$V(\hat{N}) = E_C(\hat{N} - n_x)^2, \tag{4}$$

where $E_C = \frac{e^2}{2C}$ is the charging energy, $en_x = C_L V_L + C_R V_R + C_g V_g$, $C = C_L + C_R + C_g$, and V_s, C_s $(s = L, R, g)$ are the voltages and capacitances of the circuit according to Fig. 1. $\hat{N}$ denotes the excess particle number operator on the metallic island. The charge transfer processes due to tunneling are described by

$$H_T = \sum_{r=L,R} \sum_{kln} (T^{rn}_{kl} a^\dagger_{krn} c_{ln} e^{-i\hat{\phi}} + \text{c.c.}), \tag{5}$$

where T^{rn}_{kl} are the tunneling matrix elements and $e^{\pm i\hat{\phi}}$ changes the excess particle number on the island by ± 1. $\hat{\phi}$ is the phase operator canonical conjugate to $\hat{N}$, i.e., $[\hat{\phi}, \hat{N}] = i$. The states $N = 0, \pm 1, \pm 2, \ldots$, correspond to discrete charge states with Coulomb energy $V(N)$ given by (4). They are treated independently of the degrees of freedom described by the field operators $c_{ln}, c^\dagger_{ln}$.[11] This is a good approximation when the total charge on the is-

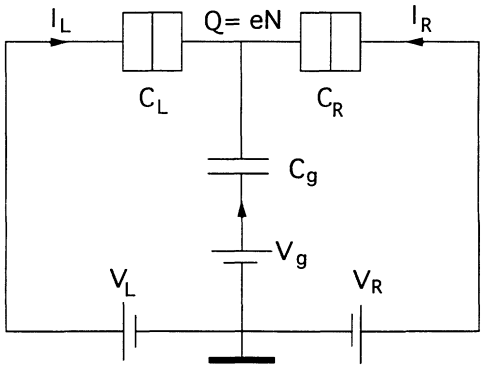

FIG. 1. Equivalent circuit for the SET transistor.

land (excess charge plus background charge) is very large which is certainly the case here due to the dense level spectrum of the metallic island.

The two leads as well as the island are treated as large equilibrium reservoirs which are not affected significantly by coherent tunneling processes where only a small number of electrons are involved. Thus, we describe the electrons in these three "reservoirs" by Fermi distribution functions $f_i(E) = 1/\exp[\beta(E-\mu_i)+1]$ $(i = L, R, I)$ with fixed chemical potentials μ_i or equivalently by the grand canonical density matrix,

$$\rho_R^0 = \frac{1}{Z_R^0} \exp\left(\beta \sum_{i=L,R,I} (H_i - \mu_i \hat{N}_i)\right), \tag{6}$$

where $\beta = 1/T$ and $\hat{N}_i$ are the number of electrons in the leads and the island, respectively. In the following, we will always set the chemical potential μ_I of the island to be zero.

The coupling between the reservoirs and the discrete charge states via (5) changes the probability P_N for a certain excess particle number N on the island. To calculate the distribution $P_N(t)$ at time t, we start from an arbitrary initial distribution $P_N^0 = P_N(t_0)$ at time t_0 and write formally,

$$P_N(t) = \langle (|N\rangle\langle N|)(t)\rangle_{\rho_0}, \tag{7}$$

where $\rho_0 = \rho_R^0 \hat{P}^0$ is the initial density matrix of the whole system, $\hat{P}^0$ is a diagonal operator with matrix elements $P_N^0 = \langle N|\hat{P}^0|N\rangle$ and $|N\rangle$ denote the discrete charge states.

The stationary distribution follows from

$$P_N^{\rm st} = \lim_{t\to\infty} P_N(t) = \lim_{t_0\to-\infty} P_N(0), \tag{8}$$

and will turn out to be independent of the initial choice for P_N^0. Note that this distribution is not the equilibrium one if the chemical potentials $\mu_{L/R}$ of the leads are different. The average charge of the island can be calculated from

$$\bar{N} = \sum_N N\, P_N^{\rm st}, \tag{9}$$

which is an experimentally measurable quantity via the electrostatic potential of the island.

The current flowing through the barriers $r = L/R$ is defined by $I_r(t) = e\frac{d}{dt}\langle \hat{N}_r(t)\rangle_{\rho_0}$. After a straightforward calculation, one obtains

$$I_r(t) = 2e\,\mathrm{Im}\left\{\sum_{kln} T_{kl}^{rn} \langle (a_{krn}^\dagger c_{ln} e^{-i\hat{\phi}})(t)\rangle_{\rho_0}\right\}, \tag{10}$$

and for the stationary current,

$$I_r^{\rm st} = \lim_{t\to\infty} I_r(t) = \lim_{t_0\to-\infty} I_r(0). \tag{11}$$

In Sec. IV [see (45)], we will show that the stationary current can also be related to the following two real-time correlation functions:

$$C^>(t,t') = -i\langle e^{-i\hat{\phi}(t)} e^{i\hat{\phi}(t')}\rangle_{\rho_0}, \tag{12}$$

$$C^<(t,t') = i\langle e^{i\hat{\phi}(t')} e^{-i\hat{\phi}(t)}\rangle_{\rho_0}, \tag{13}$$

which are independent quantities since we do not assume equilibrium here. In the stationary limit, i.e., $t_0 \to -\infty$, the correlation functions depend only on the relative time difference $\tau = t - t'$ and we can define the Fourier transform,

$$C^>(\omega) = \int d\tau\, e^{i\omega\tau} C^>(\tau) \tag{14}$$

and analog for $C^<(\omega)$. From a theoretical point of view, an interesting quantity is also the spectral density,

$$A(\omega) = \frac{1}{2\pi i}[C^<(\omega) - C^>(\omega)], \tag{15}$$

which describes the charge excitations of the system. At the end of Sec. IV, we will see that within our approximations all quantities of interest like the probability $P_N^{\rm st}$, the current $I_{L/R}^{\rm st}$, and the correlation functions $C^>, C^<$ can be related to the spectral density. Thus, its specific form which is related to energy renormalization and finite lifetime broadening effects will be the central point of our analysis.

III. DIAGRAMMATIC TECHNIQUE

To start with, we consider the probability distribution (7) and write it in the form

$$P_N(t) = \sum_{N'} P_{N'}^0\, \mathrm{Tr}_R\, \rho_R^0\, \langle N'|\, T^{(+)} e^{i\int_{t_0}^t d\tau H_T(\tau)_0}\, |N\rangle$$

$$\times \langle N|\, T^{(-)} e^{-i\int_{t_0}^t d\tau H_T(\tau)_0}\, |N'\rangle, \tag{16}$$

where Tr_R is the trace over all reservoirs, $T^{(+)}$ ($T^{(-)}$) are the (anti-) time-ordering operators, and $H_T(\tau)_0$ denotes the tunneling part of the Hamiltonian (2) in interaction representation with respect to H_0. Note that the Coulomb interaction V is included here in H_0 and will be treated exactly in the following. Equation (16) has also been used as a starting point by other authors, e.g., by Feynman and Vernon[24] (see, also, Ref. 25) for a system coupled to a heat bath or by Eckern, Schön, and Ambegaokar[26] for the same system we are considering here. After integrating out the reservoirs within a real-time path integral representation, these authors obtained an effective action where the two propagators occurring in Eq. (16) are coupled to each other. Expanding the exponential of this action in terms of the tunneling, one can arrive at a graphical language in real-time space.[5]

In this work, we will use an alternative approach which is easily generalizable to other systems as well, as, e.g., quantum dots, Anderson and Kondo models, etc.[36] The procedure is first to expand the propagators in H_T by

$$T^{(\pm)} e^{\pm i \int_{t_0}^{t} d\tau H_T(\tau)_0}$$

$$= \sum_{m=0}^{\infty} (\pm i)^m \int_{t_0}^{t} d\tau_1 \int_{t_0}^{\tau_1} d\tau_2 \cdots \int_{t_0}^{\tau_{n-1}} d\tau_n \; T^{(\pm)} \times \{H_T(\tau_1) \cdots H_T(\tau_n)\}, \tag{17}$$

and, in a second step, insert the form (5) for H_T and apply Wick's theorem with respect to the reservoir field operators $a_{krn}^{(\dagger)}$ and $c_{ln}^{(\dagger)}$. This is possible since H_0 is bilinear in these operators. As a consequence, the vertices corresponding to the charge transfer operators $e^{\pm i\hat{\phi}}$ become coupled by reservoir lines, either from the two leads or the island. This is indicated in a graphical language by solid lines for the leads and wiggly lines for the island as shown in Fig. 2. There the upper (lower) horizontal line corresponds to the forward (backward) propagator and the vertices change the discrete charge states as indicated by the particle numbers associated with the horizontal lines. The two charge states at the left end of the diagram at time t_0 are the same and lead to the factor $P_{N'}^0$ from the initial probability distribution. The two charge states at the right end at time t are identical to N if we want to calculate $P_N(t)$. Graphically we indicate the relationship of the upper and lower states at the two end points by external vertices given by $\hat{P}^0$ and $|N\rangle\langle N|$. All the other vertices are called internal vertices. Furthermore, we assign to each line a certain energy, the Coulomb energy $V(N)$ to the horizontal lines and the energies ϵ (E) to the lead (island) lines. The rules to translate a certain diagram in time space are the following ones.

(1) Assign a factor $e^{-ix_j\tau_j}$ to each vertex where τ_j is the time variable and x_j is the difference of the energies entering the vertex minus all energies leaving the vertex.

(2) To each loop formed by $2s$ reservoir lines, we assign a factor

$$\alpha_{r_1 \ldots r_s}^{\sigma_1,\ldots,\sigma_s,\eta_1,\ldots,\eta_s}(\epsilon_1 \ldots \epsilon_s, E_1 \ldots E_s)$$

$$= \sum_{n} \sum_{l_1 \cdots l_s} \Gamma_{l_1 l_2}^{r_1 n \sigma_1 \eta_1}(\epsilon_1, E_1) \Gamma_{l_2 l_3}^{r_2 n \sigma_2 \eta_2}(\epsilon_2, E_2) \times \cdots \Gamma_{l_s l_1}^{r_s n \sigma_s \eta_s}(\epsilon_s, E_s), \tag{18}$$

where $\epsilon_1, \ldots, \epsilon_s$ and $E_1, \ldots, E_s$ are the energies associated to the lead and island electrons, respectively, ordered in the direction of the loop, $r_j = L/R$ specifies the left or the right lead and each sign $\sigma_j, \eta_j = \pm$ indicates whether the reservoir line with energy ϵ_j, E_j runs to a larger $(-)$ or a lower $(+)$ time with respect to the closed time path formed by the two propagators. The quantities Γ are defined by

$$\Gamma_{ll'}^{rn\sigma\eta}(\epsilon, E) = \sum_{k} T_{kl}^{rn} T_{kl'}^{rn*} \delta(\epsilon - \epsilon_{kn}^{r}) \times \delta(E - \epsilon_{ln}) f_r^{\sigma}(\epsilon) f_I^{\eta}(E), \tag{19}$$

where $f_i^{+} = f_i$ $(i = L, R, I)$ is the Fermi distribution function and $f_i^{-} = 1 - f_i$.

(3) The prefactor is given by $(-i)^M (-1)^m (-1)^c$, where M is the total number of internal vertices, m the number of internal vertices on the backward propagator, and c the number of crossings of reservoir lines. Finally, one has to integrate over all time variables τ_j from t_0 to t and over all energy variables of the reservoir lines.

For the current (10) and the correlation functions (12,13), the procedure is completely analog, the only difference is that the external vertices have to be changed. As can be seen from Fig. 3 one has to introduce an external vertex with two reservoir lines at the right end of the diagram to calculate the current, and two external vertices to calculate the correlation functions.

So far, the diagrammatic rules are formulated in time space which is not the most convenient one to calculate stationary transport properties. Therefore, using (8) and (11), we set $t = 0$ and $t_0 = -\infty$ in every diagram for $P_N(t)$ and $I_r(t)$ and evaluate the time integrals analytically for a given fixed ordering of all time variables by using the identity

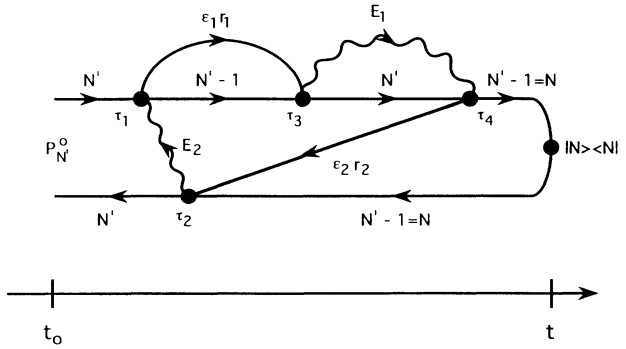

FIG. 2. Example of a diagram in time space for the probability $P_N(t)$. Time is increasing from left to right. The dots represent the vertices which are connected by horizontal lines (propagators), solid lines (leads) or wiggly lines (island). ϵ_j, E_j are the corresponding energies, r_j are the lead indices, and N denotes the excess particle number.

$$\int_{-\infty}^{0} d\tau_1 \int_{\tau_1}^{0} d\tau_2 \cdots \int_{\tau_{M-1}}^{0} d\tau_M \, e^{-ix_1\tau_1} e^{-ix_2\tau_2} \cdots e^{-ix_M\tau_M} e^{\eta\tau_1} = i^M \frac{1}{x_1 + i\eta} \frac{1}{x_1 + x_2 + i\eta} \cdots \frac{1}{x_1 + x_2 + \cdots + x_M + i\eta}, \tag{20}$$

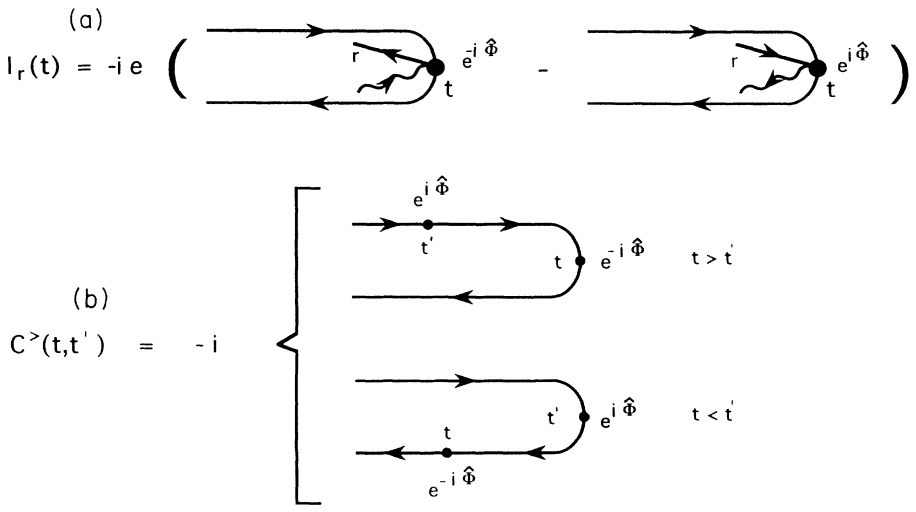

FIG. 3. Graphical representation of (a) the current I_r through lead r and (b) the correlation functions $C^>, C^<$ in time space. The dots indicate the external vertices. Further internal vertices together with their connections are not indicated.

where $e^{\eta\tau_1}$ $(\eta \to 0^+)$ is a convergence factor which is related to the adiabatic turn on of the coupling part H_T. The rules in energy space are as follows.

(1) For each auxiliary vertical line which does not cut any vertex and has always a vertex to its left, we assign a resolvent $\frac{1}{\Delta E + i\eta}$, where ΔE is the difference of all energies crossing the vertical line from right to left minus all energies crossing it from left to right (see Fig. 4).

(2) For each loop we assign the same factor as given by Eq. (18).

(3) The prefactor is given by $(-1)^m(-1)^c$, where m is the total number of internal vertices on the backward propagator and c the number of crossings of reservoir lines. Furthermore, if we are calculating the current, we have to multiply with an additional factor $-ie$ and we have to assign a factor -1 if the external vertex to the right has an incoming lead line.

For the Fourier transform (14) of the correlation functions, we write

$$C^>(\omega) = \int_{-\infty}^{0} d\tau \left[e^{-i\omega\tau} \lim_{t_0 \to -\infty} C^>(0,\tau) + e^{i\omega\tau} \lim_{t_0 \to -\infty} C^>(\tau,0) \right], \quad (21)$$

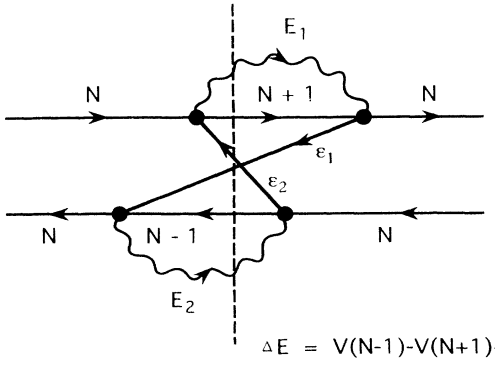

FIG. 4. Graphical determination of the energy denominators. The energies of all lines contribute to ΔE which are cut by an auxiliary vertical line.

and, again, calculate all time integrals analytically by using (20) and fixing the time ordering of all time variables including the integration variable τ. Rule 1 has then to be supplemented by rule 4.

(4) If an auxiliary vertical line lies between the two external vertices, we have to add $\pm\omega$ to the energy difference ΔE when the vertex $e^{\pm i\hat{\phi}}$ lies to the left of the auxiliary line (see Fig. 5). If we imagine a virtual line which connects the two external vertices from $e^{-i\hat{\phi}}$ to $e^{i\hat{\phi}}$ and assign an energy ω to it, we can simulate the same by, consequently, applying rule 1 including this virtual line. The graphical representation of $C^>(\omega)$ and $C^<(\omega)$ in energy space is given in Fig. 6.

IV. PHYSICAL PROCESSES

Usually, tunneling processes within the SET transistor are described by a classical Master equation,[1,5–8,37]

$$\dot{P}_N^{(0)}(t) = \sum_{N' \neq N} \left[P_{N'}^{(0)}(t)\gamma_{N'N} - P_N^{(0)}(t)\gamma_{NN'} \right], \quad (22)$$

where $\gamma_{N'N}$ are classical transition rates calculated by the golden rule in second-order perturbation theory in H_T,

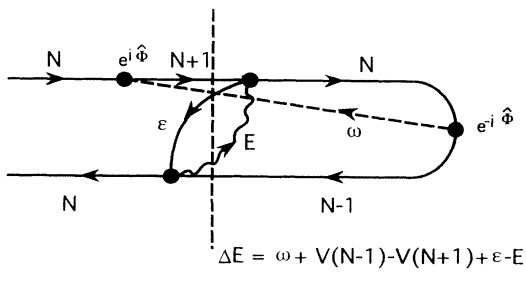

FIG. 5. If an auxiliary vertical line cuts the virtual line connecting the external vertices, the energy ω contributes to the energy denominators.

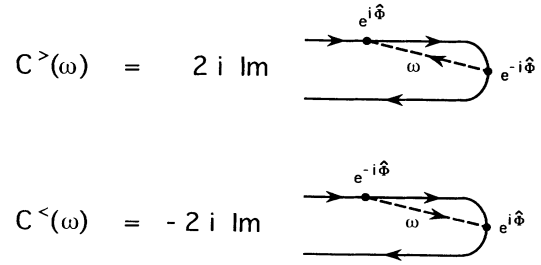

FIG. 6. Graphical representation of the correlation functions in energy space.

$$\gamma_{N'N} = 2\pi \sum_r \left[\alpha_r^-(\Delta_N)\delta_{N',N+1} + \alpha_r^+(\Delta_{N-1})\delta_{N',N-1}\right]. \tag{23}$$

Here, $\Delta_N = V(N+1) - V(N)$ is the change of the Coulomb energy if we increase the excess particle number by 1 and

$$\alpha_r^{\pm}(\omega) = \int dE\, \alpha_r^{\pm,\mp}(\omega + E, E) \tag{24}$$

are the transition rates for tunneling in and out processes. Assuming constant tunneling matrix elements $T^{rn} = T^{rn}_{kl}$ and neglecting the energy dependences of the density of states $\rho_r^n(\epsilon), \rho_I^n(E)$ in the leads and the island, we obtain the well-known expressions,

$$\alpha_r^{\pm}(\omega) = (\omega - \mu_r)\alpha_0^r\, n_r^{\pm}(\omega), \tag{25}$$

where

$$\alpha_0^r = \sum_n |T^{rn}|^2 \rho_r^n \rho_I^n = \frac{1}{4\pi^2}\frac{R_K}{R_T^r} \tag{26}$$

is the ratio of the quantum resistance $R_K = \frac{h}{e^2}$ to the tunneling resistance R_T^r of barrier r, $n_r^+(\omega) = 1/\{\exp[\beta(\omega - \mu_r)] - 1\}$ is the Bose function and $n_r^- = 1 + n_r^+$. Furthermore, we introduce the notations $\alpha_0 = \sum_r \alpha_0^r$, $\alpha^{\pm}(\omega) = \sum_r \alpha_r^{\pm}(\omega)$, $\alpha_r(\omega) = \alpha_r^+(\omega) + \alpha_r^-(\omega)$, and $\alpha(\omega) = \alpha^+(\omega) + \alpha^-(\omega)$.

Physically, the Master equation (22) describes sequences of uncorrelated lowest-order processes (sequential tunneling) where each single process describes one electron entering or leaving the island. Retardation effects and higher-order correlated tunneling processes are neglected within this approach. Writing (22) in the form

$$\dot{P}_N^{(0)}(t) = \sum_{N'} P_{N'}^{(0)}(t)\bar{\gamma}_{N'N}, \tag{27}$$

with $\bar{\gamma}_{N'N} = \gamma_{N'N} - \delta_{N'N}\sum_{N''}\gamma_{NN''}$, we will now show that the exact kinetic equation has the form

$$\dot{P}_N(t) = \sum_{N'} \int_{t_0}^{t} dt'\, P_{N'}(t')\tilde{\Sigma}_{N'N}(t'-t), \tag{28}$$

where non-Markovian effects are included and $\tilde{\Sigma}$ denotes the sum of all possible correlated processes. For the stationary solution $P_N^{\rm st}$, this gives

$$0 = \sum_{N'} P_{N'}^{\rm st}\Sigma_{N'N}, \tag{29}$$

where $\Sigma_{N'N} = i\int_{-\infty}^{0} d\tau \tilde{\Sigma}_{N'N}(\tau)$. This equation can immediately be obtained by using our diagrammatic technique in energy space. The self-consistent equation for $P_N^{\rm st}$ is shown in Fig. 7. Here, Σ is defined graphically as the sum of all possible irreducible self-energy diagrams, which are defined such that any vertical line cutting them will cross some reservoir line (see Fig. 8). According to our diagrammatic rules 1, 2, and 3 in energy space, the equation corresponding to Fig. 7 reads

$$P_N^{\rm st} = P_N^0 + \sum_{N'} P_{N'}^{\rm st}\Sigma_{N'N}\frac{1}{i\eta}. \tag{30}$$

Multiplying with $i\eta$ and performing the limit $\eta \to 0^+$, we arrive at (29) and can identify the sum of all possible correlated tunneling processes diagrammatically by the irreducible self-energy Σ. Furthermore, the solution of Eq. (29) is independent of the initial choice for P_N^0 which has dropped out of Eq. (30) by performing the limit $\eta \to 0^+$. In the same way, one can also set up a self-consistent equation in time space to get the time-dependent kinetic equation (28).

By moving the last vertex to the right of each diagram of Σ up or down, one can easily show that

$$\sum_{N'} \Sigma_{NN'} = 0, \tag{31}$$

which provides the possibility to write Eq. (29), also, in the form

$$0 = \sum_{N' \neq N} \left(P_{N'}^{\rm st}\Sigma_{N'N} - P_N^{\rm st}\Sigma_{NN'}\right). \tag{32}$$

This has the form of a balance equation for each charge state $|N\rangle$. Furthermore, by changing the vertical position of all vertices and the direction of all reservoir lines one can easily see that $\Sigma_{N'N}$ is purely imaginary, i.e., there exists a real solution of (29) and (32).

Calculating $\Sigma_{N'N}$ in first order in α_0 (see Fig. 9), we get

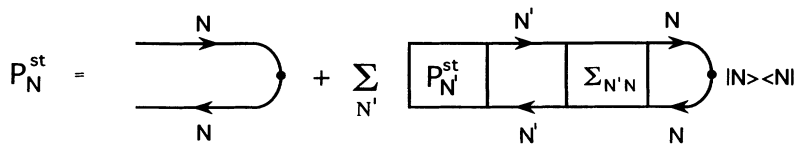

FIG. 7. Self-consistent equation for the stationary probability $P_N^{\rm st}$. The self-energy Σ denotes the sum of all irreducible diagrams which cannot be cut into two parts by an arbitrary vertical line.

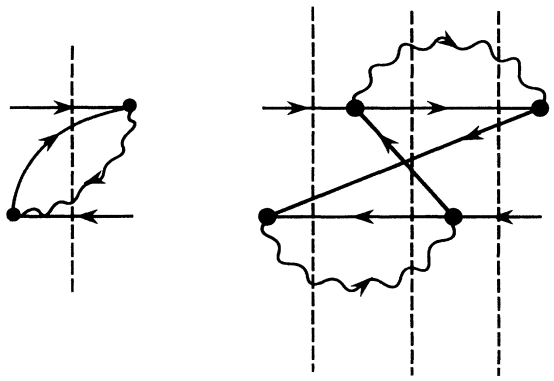

FIG. 8. Examples for irreducible diagrams. An arbitrary vertical line will always cut through some reservoir line.

$$\Sigma^{(1)}_{N+1,N} = 2\pi i\alpha^{-}(\Delta_N)\ ,\ \Sigma^{(1)}_{N-1,N} = 2\pi i\alpha^{+}(\Delta_{N-1})\,, \tag{33}$$

which, after insertion in Eq. (29), leads to the classical result (27) in the stationary limit.

Before starting to include higher-order processes in Σ, we will introduce two important approximations which will simplify the following analysis considerably.

First, we assume that the number Z of transverse channels is very large. Since each loop contribution (18) is proportional to $Z\Gamma^s$, this has the consequence that all loops with $s = 1$ will dominate in each given perturbation order in Γ. Thus, we can restrict ourselves to the loops with two reservoir lines which give the contribution $\alpha_r^{\pm,\mp}(\epsilon, E)$. Since the rest of the diagram depends only on $\omega = \epsilon - E$, we can integrate $\alpha_r^{\pm,\mp}(\omega + E, E)$ over E and get the contribution $\alpha_r^{\pm}(\omega)$ defined by (24,25). Furthermore, we represent all loops with two reservoir lines from now on graphically by single solid lines with one energy variable ω (see Fig. 10).

Secondly, for a large charging energy E_C, we will use the two charge state approximation which means that only the two charge states with $N = 0, 1$ will be considered. This is possible when the energy difference of the two charge states $\Delta_0 = V(1) - V(0)$ and the bias voltage $V = V_L - V_R$ are small compared to the charging energy.

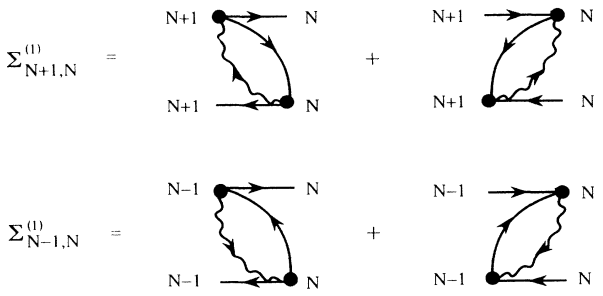

FIG. 9. First-order diagrams for Σ which correspond to the classical transition rates.

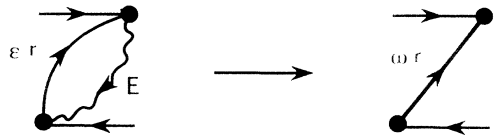

FIG. 10. Replacement of a loop consisting of one lead and one island line by a single solid line. The arrow direction is the same as of the lead line.

The classical approach breaks down for low temperatures or for large values for the dimensionless conductance α_0. Specifically, we will see in Sec. V that the classical master equation is valid for $\alpha_0 \ln(\frac{E_C}{2\pi T}) \ll 1$. To go beyond this regime we consider now higher-order correlated tunneling processes in Σ. Figure 11 shows an example in second order in α_0 which corresponds to inelastic electron cotunneling processes[16,17] when the leads r and r' are different. Here, one electron enters the island from lead r, the system stays in a virtual intermediate charge state with $N = 1$ and, finally, another electron leaves the island via lead r'. However, the calculation of all second-order diagrams for $\Sigma_{01} = -\Sigma_{00}$ or $\Sigma_{10} = -\Sigma_{11}$ is plagued by several irregular integrals which occur since the complete self-energy depends nonanalytically on α_0. Thus, instead of regularizing the integrals by unclear procedures, we will directly perform a nonperturbative resummation of higher-order diagrams and discuss the second-order result as a limiting case at the end. By this, we are also able to clarify certain singularities which are present in the usual expressions for inelastic electron cotunneling.[16,17] Furthermore, we are able to go beyond the cotunneling theory and can investigate the influence of resonant tunneling processes which will modify the classical result of sequential tunneling significantly if $\alpha_0 \ln(\frac{E_C}{2\pi T}) \sim 1$.

A very illustrative example of a resonant tunneling process is shown in Fig. 12. Here, the charge of the island is alternating between 0 and 1 via an infinite number of intermediate virtual states. The electrons going back and forth between the leads and the island are all different since we have assumed a large number of transverse channels. This is in contrast to the usual mechanism of resonant tunneling where only one level of the island is involved. Of course, the diagram of Fig. 12 is not the only one which is important to describe higher-order processes. In order to get a systematic criterion which diagrams might be the relevant ones, we remember that the states corresponding to the upper and lower hori-

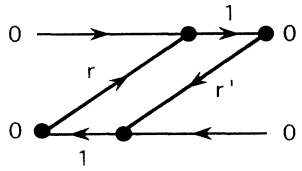

FIG. 11. Second-order diagram for Σ_{00} which contributes to inelastic electron cotunneling when the two leads r and r' are different.

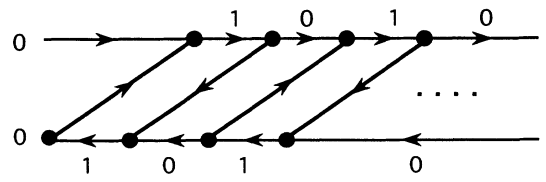

FIG. 12. Higher-order diagrams which contribute to resonant tunneling.

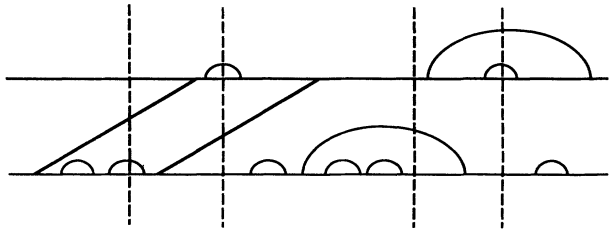

FIG. 13. Example of a diagram which is taken into account. All vertical lines cut at most through two solid lines. The cut through the two horizontal lines is trivial and is not counted.

zontal lines are matrix elements of the density matrix. Before integrating out the reservoir degrees of freedom, we can also follow up the states within the leads and the island. Our criterion now is that we take into account only those matrix elements of the total density matrix, i.e., reservoirs plus charge states, which differ at most by one electron-hole pair excitation in the leads or (equivalently) in the island. Graphically this means that any vertical line will at most cut through two solid lines each representing a pair of one lead and one island line (see Fig. 13 for examples). The sum of all these diagrams can be represented as shown in Figs. 14–16. We get for $N = 0, 1$,

$$\Sigma_{N1} = -2i \,\mathrm{Im} \int d\omega \sum_r \phi_N^r(\omega), \tag{34}$$

together with the self-consistent equation,

$$\phi_N^r(\omega) = \Pi(\omega) \Big[\alpha_r^+(\omega)\delta_{N0} - \alpha_r^-(\omega)\delta_{N1} - \alpha_r(\omega) \int d\omega' \frac{1}{\omega - \omega' + i\eta} \sum_{r'} \phi_N^{r'}(\omega')^* \Big], \tag{35}$$

where

$$\Pi(\omega) = \frac{1}{\omega - \Delta_0 - \sigma(\omega)}, \quad \sigma(\omega) = \int d\omega' \frac{\alpha(\omega')}{\omega - \omega' + i\eta}. \tag{36}$$

Defining

$$\psi_+(\omega) = \frac{\phi_0^r(\omega)}{\alpha_r(\omega)} - \frac{\alpha_r^+(\omega)}{\alpha_r(\omega)}\Pi(\omega) + \frac{\alpha^+(\omega)}{\alpha(\omega)}\Pi(\omega), \tag{37}$$

$$\psi_-(\omega) = \frac{\phi_1^r(\omega)}{\alpha_r(\omega)} + \frac{\alpha_r^-(\omega)}{\alpha_r(\omega)}\Pi(\omega) - \frac{\alpha^-(\omega)}{\alpha(\omega)}\Pi(\omega), \tag{38}$$

which are quantities independent of r due to Eq. (35), we obtain the integral equation,

$$[\omega - \Delta_0 - \sigma(\omega)]\,\psi_\pm(\omega) = \pm\frac{\alpha^\pm(\omega)}{\alpha(\omega)} - \int d\omega' \frac{\alpha(\omega')}{\omega - \omega' + i\eta}\psi_\pm(\omega')^*. \tag{39}$$

Since $\mathrm{Im}\,\sigma(\omega) = -\pi\alpha(\omega)$, the solution of this integral equation is

$$\mathrm{Im}\,\psi_\pm(\omega) = \mp\pi\frac{\lambda_\pm}{\lambda}|\Pi(\omega)|^2, \tag{40}$$

where

$$\lambda_\pm = \int d\omega \alpha^\pm(\omega)|\Pi(\omega)|^2, \qquad \lambda = \int d\omega |\Pi(\omega)|^2 \tag{41}$$

and the real part of $\psi_\pm(\omega)$ can be obtained from (39) and the Kramers-Kronig relation although it is not necessary for the following. From Eq. (40), we can calculate $\mathrm{Im}\,\phi_N^r(\omega)$ with the help of (37,38) and obtain from Eq. (34) a nonperturbative expression for the transition matrix elements,

$$\Sigma_{01} = -\Sigma_{00} = 2\pi i\frac{\lambda_+}{\lambda}, \tag{42}$$

$$\Sigma_{10} = -\Sigma_{11} = 2\pi i\frac{\lambda_-}{\lambda}. \tag{43}$$

Inserting these quantities in the kinetic equation (32) and solving it, we obtain for the stationary probabilities,

$$P_0^{\mathrm{st}} = \lambda_- \ , \ P_1^{\mathrm{st}} = \lambda_+ , \tag{44}$$

where $\lambda_+ + \lambda_- = 1$ has been used which ensures the normalization $P_0^{\mathrm{st}} + P_1^{\mathrm{st}} = 1$. Furthermore, both probabilities are strictly positive. The solution (44) is the final result for the density matrix and will be discussed in detail in Sec. V B.

In order to calculate the stationary current I_r^{st}, we relate it to the correlation functions $C^>(\omega)$ and $C^<(\omega)$ as indicated in Fig. 17 which gives

$$I_r^{\mathrm{st}} = -ie \int d\omega \left\{ \alpha_r^+(\omega)C^>(\omega) + \alpha_r^-(\omega)C^<(\omega) \right\}. \tag{45}$$

This relation is exact in the limit of a very large number of transverse channels. Otherwise, the current will also depend on correlation functions involving more than two charge transfer operators $e^{\pm i\hat{\phi}}$.

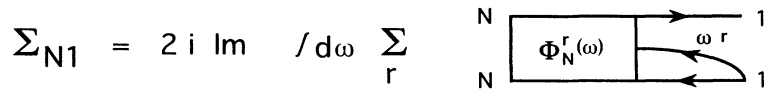

FIG. 14. Graphical representation of the self-energy Σ_{N1} within our approximation.

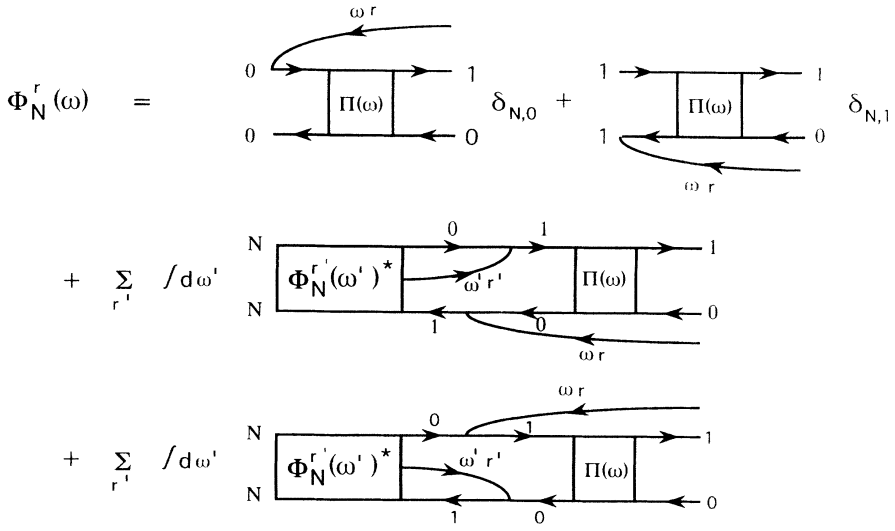

FIG. 15. Self-consistent equation for $\phi^r_N(\omega)$.

The correlation functions can now be calculated from the diagrams shown in Fig. 18, where we have used the same criterion as for the calculation of the density matrix with one exception. If a vertical line lies between the external vertices, we allow for a cut through at most one solid line. Thereby, we have used the fact that such a vertical line will, in addition, always cut the virtual line connecting the external vertices. The sum of all these diagrams gives

$$C^>(\omega) = 2i\,\mathrm{Im}\Bigg\{ P_0^{\mathrm{st}}\,\Pi(\omega) - \sum_{N=0,1}\sum_{r=L/R} P_N^{\mathrm{st}} \int d\omega' \frac{\phi_N^r(\omega')^*}{\omega-\omega'+i\eta}\Pi(\omega)\Bigg\}, \tag{46}$$

$$C^<(\omega) = -2i\,\mathrm{Im}\Bigg\{ -P_1^{\mathrm{st}}\Pi(\omega)^* + \sum_{N=0,1}\sum_{r=L/R} P_N^{\mathrm{st}} \int d\omega' \frac{\phi_N^r(\omega')}{\omega'-\omega+i\eta}\Pi(\omega)^*\Bigg\}, \tag{47}$$

which yields with Eqs. (37), (38), (40), and (44),

$$C^>(\omega) = -2\pi i\,\alpha^-(\omega)\,|\Pi(\omega)|^2, \tag{48}$$

$$C^<(\omega) = 2\pi i\,\alpha^+(\omega)\,|\Pi(\omega)|^2. \tag{49}$$

Furthermore, we obtain for the spectral density (15),

$$A(\omega) = \alpha(\omega)\,|\Pi(\omega)|^2, \tag{50}$$

which is normalized to unity $\int d\omega A(\omega) = 1$.

Using (41), (44), (45), (48), (49), and (50) we can express all our final results in terms of the spectral density,

$$P_0^{\mathrm{st}} = \int d\omega \frac{\sum_r \alpha_r(\omega) f_r^-(\omega)}{\alpha(\omega)} A(\omega), \tag{51}$$

$$P_1^{\mathrm{st}} = \int d\omega \frac{\sum_r \alpha_r(\omega) f_r^+(\omega)}{\alpha(\omega)} A(\omega), \tag{52}$$

$$I_r^{\mathrm{st}} = \frac{e}{h} 4\pi^2 \int d\omega \sum_{r'} \frac{\alpha_{r'}(\omega)\alpha_r(\omega)}{\alpha(\omega)} A(\omega)[f_{r'}^+(\omega) - f_r^+(\omega)], \tag{53}$$

$$C^>(\omega) = -2\pi i \frac{\sum_r \alpha_r(\omega) f_r^-(\omega)}{\alpha(\omega)} A(\omega), \tag{54}$$

$$C^<(\omega) = 2\pi i \frac{\sum_r \alpha_r(\omega) f_r^+(\omega)}{\alpha(\omega)} A(\omega), \tag{55}$$

where we have used the relation $\alpha_r^\pm(\omega) = \alpha_r(\omega) f_r^\pm(\omega)$.

These results satisfy conservation laws and sum rules. Current is conserved, i.e., $\sum_r I_r^{\mathrm{st}} = 0$, and is zero in the equilibrium case when $\mu_r = 0$. All probabilities are positive, the spectral density is normalized to unity and

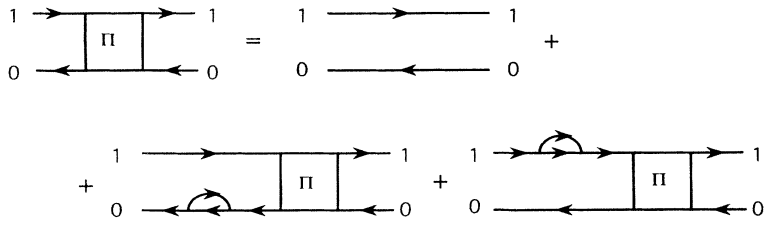

FIG. 16. Definition of Π. To each energy denominator one has to add ω in order to obtain $\Pi(\omega)$.

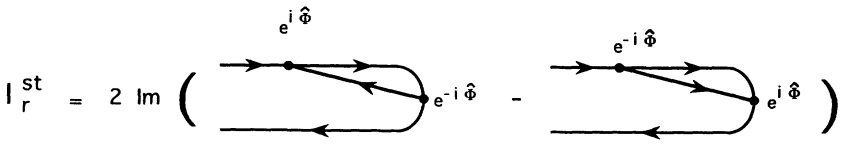

FIG. 17. Graphical representation of the relation between the current and the correlation functions. Here, the line connecting the external vertices is a real one. All the other internal vertices are not indicated.

we get the correct relationships between the correlation functions and the spectral density in the equilibrium case. The classical result can be recovered from (51)–(55) if we use the lowest-order approximation in α_0 for the spectral density,

$$A^{(0)}(\omega) = \delta(\omega - \Delta_0). \tag{56}$$

Thus, we can conclude this section by the observation that quantum fluctuation effects due to energy renormalization and broadening manifest themselves in the spectral density via the real and imaginary part of the self-energy $\sigma(\omega)$ given in Eq. (36). This will be the main subject of the detailed discussion in the next section.

V. RESULTS AND APPLICATIONS

A. The spectral density

Using Eq. (25) one can evaluate the self-energy $\sigma(\omega)$ given by Eq. (36) as

$$\sigma(\omega) = -\sum_r \alpha_0^r \left[R(\omega - \mu_r) + iI(\omega - \mu_r)\right], \tag{57}$$

where

$$R(\omega) = D(\omega)\omega\left[\psi\left(\frac{E_C}{2\pi T}\right) + \psi\left(1 + \frac{E_C}{2\pi T}\right) - 2\,\mathrm{Re}\,\psi\left(i\frac{|\omega|}{2\pi T}\right)\right], \tag{58}$$

$$I(\omega) = D(\omega)\pi\omega\,\coth\left(\frac{\omega}{2T}\right), \tag{59}$$

ψ is the digamma function and we have chosen a Lorentzian cutoff function $D(\omega) = E_C^2/(\omega^2 + E_C^2)$ with a bandwidth given by the charging energy E_C. For $E_C \gg |\omega - \mu_r| \gg T$, the self-energy $\sigma(\omega)$ behaves marginally,

$$\sigma(\omega) = -\sum_r \alpha_0^r \left[2(\omega - \mu_r)\ln\left(\frac{E_C}{|\omega - \mu_r|}\right) + i\pi|\omega - \mu_r|\right]. \tag{60}$$

Since the imaginary part is linear in ω, the broadening effects manifest themselves in a very unusual way.

We will now analyze two limiting cases, either $T \ll |\omega - \mu_r| \ll E_C$ or $|\omega - \mu_r| \leq T \ll E_C$. Furthermore, we

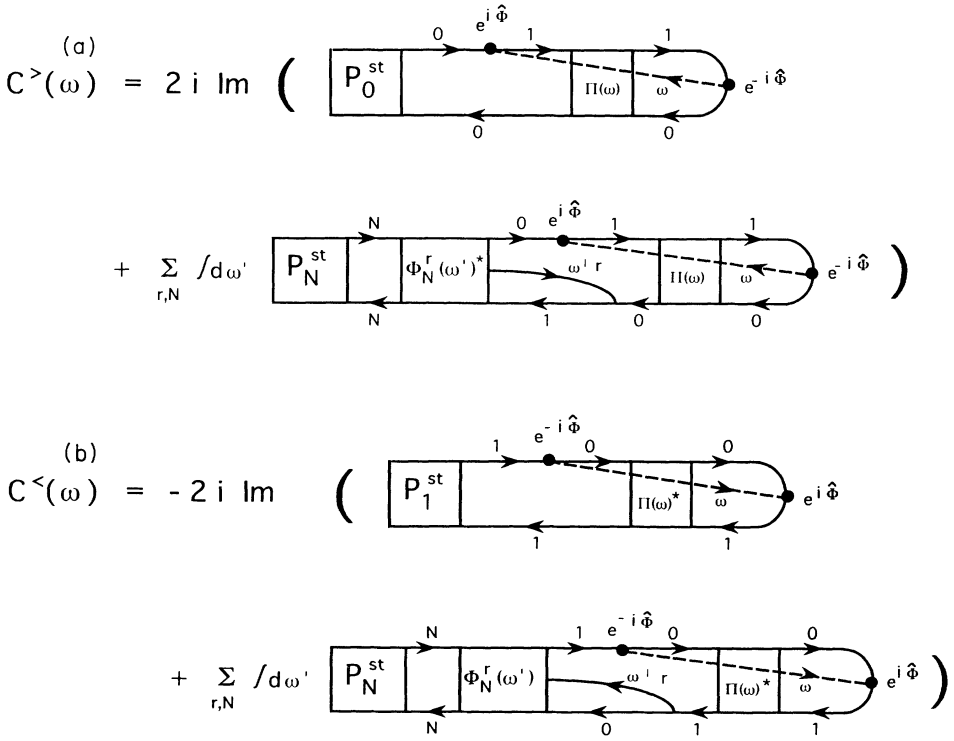

FIG. 18. Graphical representation of (a) $C^{>}(\omega)$ and (b) $C^{<}(\omega)$ within our approximation.

assume for simplicity and with regard to the applications we are discussing in Sec. V B and V C that all chemical potentials of the reservoirs are zero.

In the first case, i.e., $T \ll |\omega| \ll E_C$, we can use Eq. (60) and obtain from Eqs. (50) and (36) for the spectral density,

$$A(\omega) \cong \frac{|\omega|}{\Delta_0} \frac{\tilde{\Delta}(\omega)\tilde{\alpha}(\omega)}{[\omega - \tilde{\Delta}(\omega)]^2 + \left(\pi\tilde{\Delta}(\omega)\tilde{\alpha}(\omega)\right)^2}, \qquad T \ll |\omega| \ll E_C, \quad (61)$$

where $\tilde{\Delta}$ and $\tilde{\alpha}$ are the renormalized parameters

$$\tilde{\Delta}(\omega) = \frac{\Delta_0}{1 + 2\alpha_0 \ln\left(\frac{E_C}{|\omega|}\right)} \frac{1}{1 + \pi^2\tilde{\alpha}(\omega)^2}, \quad (62)$$

$$\tilde{\alpha}(\omega) = \frac{\alpha_0}{1 + 2\alpha_0 \ln\left(\frac{E_C}{|\omega|}\right)}. \quad (63)$$

Approximately, $A(\omega)$ will have a maximum value at $\tilde{\Delta}_0 = \tilde{\Delta}(\tilde{\Delta}_0)$ with a broadening of the order of $\pi\tilde{\Delta}_0\tilde{\alpha}_0$ where $\tilde{\alpha}_0 = \tilde{\alpha}(\tilde{\Delta}_0)$. This broadening can be neglected for $\pi\tilde{\alpha}_0 \ll 1$ and in this case, we obtain

$$\tilde{\Delta}_0 = \frac{\Delta_0}{1 + 2\alpha_0 \ln\left(\frac{E_C}{|\tilde{\Delta}_0|}\right)}, \quad \tilde{\alpha}_0 = \frac{\alpha_0}{1 + 2\alpha_0 \ln\left(\frac{E_C}{|\tilde{\Delta}_0|}\right)}, \quad (64)$$

for the renormalized gap and the renormalized dimensionless conductance. This result coincides with the renormalization group analysis in Ref. 14 and for small α_0 with Ref. 11, where $\tilde{\Delta}_0$ has been replaced by Δ_0 on the right-hand side (r.h.s.) of Eq. (64). Thus we can conclude that the leading logarithmic terms are included in our diagram series.

For $|\omega| \leq T \ll E_C$, we can approximate $R(\omega)$ by $2\omega \ln\left(\frac{E_C}{2\pi T}\right)$ and obtain

$$A(\omega) \cong \frac{\tilde{\Delta}_0}{\Delta_0} \cdot \frac{\tilde{\alpha}_0\,\omega \coth\left(\frac{\omega}{2T}\right)}{(\omega - \tilde{\Delta}_0)^2 + [\pi\tilde{\alpha}_0\,\omega \coth(\frac{\omega}{2T})]^2}, \qquad |\omega| \leq T \ll E_C, \quad (65)$$

where the renormalized parameters are now

$$\tilde{\Delta}_0 = \frac{\Delta_0}{1 + 2\alpha_0 \ln\left(\frac{E_C}{2\pi T}\right)}, \quad \tilde{\alpha}_0 = \frac{\alpha_0}{1 + 2\alpha_0 \ln\left(\frac{E_C}{2\pi T}\right)}, \quad (66)$$

which is the result (1) quoted in the Introduction. If $\tilde{\Delta}_0 \leq T$, the spectral density (65) has approximately a maximum at $\tilde{\Delta}_0$ with a broadening of the order of $\pi\tilde{\alpha}_0 T$. Again, for $\pi\tilde{\alpha}_0 \ll 1$ this broadening is small compared to $\tilde{\Delta}_0$. However, the results (65) and (66) are independent of the value of $\tilde{\Delta}_0$ and can be used always when we need the spectral density only for $|\omega| \leq T$. This is indeed the case for the calculation of the differential conductance in linear response as will be shown in Sec. V C.

As far as we are only interested in the maximum point $\tilde{\Delta}_0$ of the spectral density, we can conclude that it is given by (64) for $\tilde{\Delta}_0 \gg T$ and by (66) for $\tilde{\Delta}_0 \leq T$. This has also been proposed in Ref. 14. Furthermore, we can see here that the correct replacement to get (66) from (64) is given by $\tilde{\Delta}_0 \to 2\pi T$ on the r.h.s. of (64). Furthermore, by using our solution (50) for the spectral density, we can also describe the crossover regime from $\tilde{\Delta}_0 \leq T$ to $\tilde{\Delta}_0 \gg T$ and we are able to account correctly for the finite broadening if $\pi\tilde{\alpha}_0$ approaches unity. The latter case is not only of academic interest, since it is possible to achieve experimental parameters like $\frac{E_C}{2\pi T} \sim 3$, $\alpha_0 \sim 0.5$ (Ref. 38) which gives $\pi\tilde{\alpha}_0 \sim 0.75$ by using Eq. (66). Finally, we consider the case where $2\alpha_0 \ln\left(\frac{E_C}{2\pi T}\right) \sim 1$ but $\pi\tilde{\alpha}_0 \ll 1$. E.g., for $2\alpha_0 \ln\left(\frac{E_C}{2\pi T}\right) = 0.1$, $\pi\tilde{\alpha}_0 \ll 1$ requires $\alpha_0 \sim 0.01$ according to (66) which gives a temperature of the order of $0.001E_C$.

B. Charge fluctuations in the single-electron box

In the equilibrium case where $\mu_r = 0$, the SET transistor becomes equivalent to the single-electron box. The average excess particle number can be calculated from (9) and (52),

$$\bar{N} = \int d\omega f(\omega) A(\omega). \quad (67)$$

Within the classical approach given by Eq. (56), one obtains

$$\bar{N}^{\mathrm{cl}} = f(\Delta_0), \quad (68)$$

where the bare gap $\Delta_0 = E_C(1 - 2C_gV_g)$ can also be expressed in terms of the external gate voltage. Thus, $\bar{N}^{\mathrm{cl}}(V_g)$ shows a step at $V_g^{(0)} = \frac{C_g}{2}$ (or $\Delta_0 = 0$) which is smeared by temperature.

As can be seen from Figs. 19 and 20, there are clear deviations from the classical result if α_0 increases or if the temperature T is decreasing. To estimate this, we have neglected effects from the finite broadening, i.e., $\pi\tilde{\alpha}_0 \ll 1$, and have assumed that $\frac{E_C}{4} \mp \frac{\tilde{\Delta}_0}{2}$ give the energy of the ground state and the first excited state near the degeneracy point where $V(1) = V(0)$.[14] In this case, the partition function reads

$$Z \cong 2\,e^{-\frac{E_C}{4T}} \cosh\left(\frac{\tilde{\Delta}_0}{2T}\right), \quad (69)$$

and we obtain for the average excess particle number $\bar{N} = n_x - T\frac{\partial}{\partial\Delta_0} \ln Z$ [see Eq. (4)]

$$\bar{N} \cong \frac{1}{2}\left[1 - \frac{\partial\tilde{\Delta}_0}{\partial\Delta_0} \tanh\left(\frac{\tilde{\Delta}_0}{2T}\right)\right]. \quad (70)$$

From (64) and (66), it follows for $\tilde{\Delta}_0 \gg T$ as well as for $\tilde{\Delta}_0 \leq T$ that $\frac{\partial\tilde{\Delta}_0}{\partial\Delta_0} \cong \frac{\tilde{\Delta}_0}{\Delta_0}$, where we have used $\tilde{\alpha}_0 \ll 1$. Thus, we find

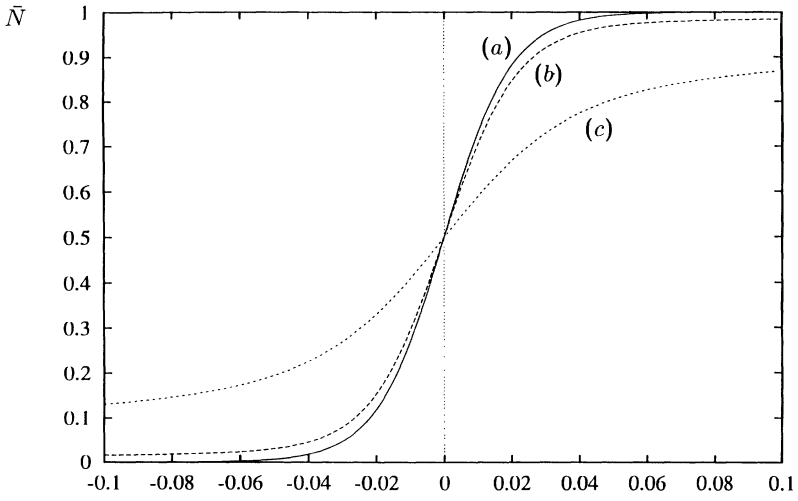

FIG. 19. Average charge as function of the gap energy for different values of α_0. $E_C = 1$, $T = 0.01$ and (a) $\alpha_0 = 0$, (b) $\alpha_0 = 0.01$, and (c) $\alpha_0 = 0.1$. Curve (a) is the Fermi distribution function which corresponds to the classical result. For increasing α_0 the deviations become more significant.

$$\bar{N} \cong \frac{1}{2}\left[1 - \frac{1}{1 + 2\alpha_0 \ln\left(\frac{E_C}{2\pi T}\right)} \times \tanh\left(\frac{\Delta_0}{2T(1 + 2\alpha_0 \ln\left(\frac{E_C}{2\pi T}\right))}\right)\right],$$

$$\tilde{\Delta}_0 \leq T, \quad \pi\tilde{\alpha}_0 \ll 1 \quad (71)$$

$$\bar{N} \cong \frac{1}{2}\left(1 - \frac{\Delta_0}{|\Delta_0|}\frac{1}{1 + 2\alpha_0 \ln\left(\frac{E_C}{|\Delta_0|}\right)}\right),$$

$$\tilde{\Delta}_0 \gg T, \quad \pi\tilde{\alpha}_0 \ll 1. \quad (72)$$

For $\tilde{\Delta}_0 \leq T$ given by Eq. (66), this means that we get significant deviations from the classical result (68) if $2\alpha_0 \ln\left(\frac{E_C}{2\pi T}\right) \sim 1$. Thus, by increasing α_0 or decreasing T, quantum fluctuations become more important. For $\tilde{\Delta}_0 \gg T$, Eq. (72) coincides with the result obtained in Ref. 11 for the $T = 0$ case.

The slope at $\Delta_0 = \tilde{\Delta}_0 = 0$ is given by

$$\left.\frac{\partial \bar{N}}{\partial \Delta_0}\right|_{\Delta_0=0} = -\frac{1}{4T[1 + 2\alpha_0 \ln\left(\frac{E_C}{2\pi T}\right)]^2}, \quad (73)$$

whereas the classical result would predict

$$\left.\frac{\partial \bar{N}}{\partial \Delta_0}\right|_{\Delta_0=0} = -\frac{1}{4T}. \quad (74)$$

Thus, we conclude that an anomalous temperature behavior of the slope of the Coulomb staircase at the degeneracy point would be an indication of coherent higher-order tunneling processes.

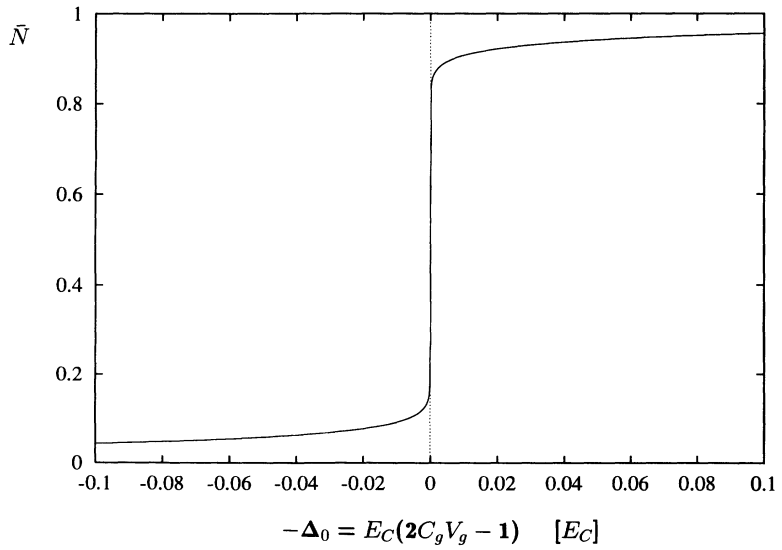

FIG. 20. Average charge as function of the gap energy at zero temperature. At finite $\alpha_0 = 0.03$ there are clear deviations from a pure step function.

Figure 21(a) shows a comparison of the fits (71), (72) with the correct result obtained from Eqs. (67) and (50). Both line shapes agree quite well for $\pi\tilde{\alpha}_0 \ll 1$, where finite lifetime broadening effects are not important. Figure 21(b) shows the same comparison for $\pi\tilde{\alpha}_0 \sim 1$ and we can see here clear differences for $\tilde{\Delta}_0 \geq T$, whereas for $\tilde{\Delta}_0 \leq T$ the approximation (71) still seems to be reasonable.

C. Conductance oscillations in the SET-transistor

In the linear response regime, we obtain for the current from (53),

$$I_R^{\rm st} = -I_L^{\rm st} = G\,(V_L - V_R), \tag{75}$$

with the conductance G given by

$$G = -\frac{e^2}{h} 4\pi^2 \int d\omega \frac{\alpha_R(\omega)\alpha_L(\omega)}{\alpha(\omega)} A(\omega) f'(\omega). \tag{76}$$

Due to the derivative of the Fermi function, the integration variable ω is in the regime $\omega \leq T$. Thus, we can use (65) and obtain after some straightforward manipulations,

$$G = \frac{e^2}{h} 2\pi^2 \frac{\tilde{\alpha}_0^R \tilde{\alpha}_0^L}{\tilde{\alpha}_0} \int d\omega \frac{\omega/T}{\sinh(\omega/T)} \times \frac{\tilde{\alpha}_0\, \omega \coth\left(\frac{\omega}{2T}\right)}{(\omega - \tilde{\Delta}_0)^2 + [\pi\tilde{\alpha}_0\, \omega \coth\left(\frac{\omega}{2T}\right)]^2}, \tag{77}$$

where $\tilde{\alpha}_0 = \tilde{\alpha}_0^R + \tilde{\alpha}_0^L$ and $\tilde{\Delta}_0$ are given by Eq. (66).

Two analytic results can be obtained from this formula. First, the maximum conductance at $\Delta_0 = \tilde{\Delta}_0 = 0$ is given by

$$G_{\rm max} = \frac{e^2}{h} 2\pi \frac{\tilde{\alpha}_0^R \tilde{\alpha}_0^L}{\tilde{\alpha}_0} \left[\frac{\pi}{2} - \arctan\left(\frac{(\pi\tilde{\alpha}_0)^2 - 1}{2\tilde{\alpha}_0 \pi}\right)\right] \tag{78}$$

and secondly, the integral of the conductance over the gap Δ_0 (or equivalently over $e^2 \frac{C_g}{C} V_g$) is equal to

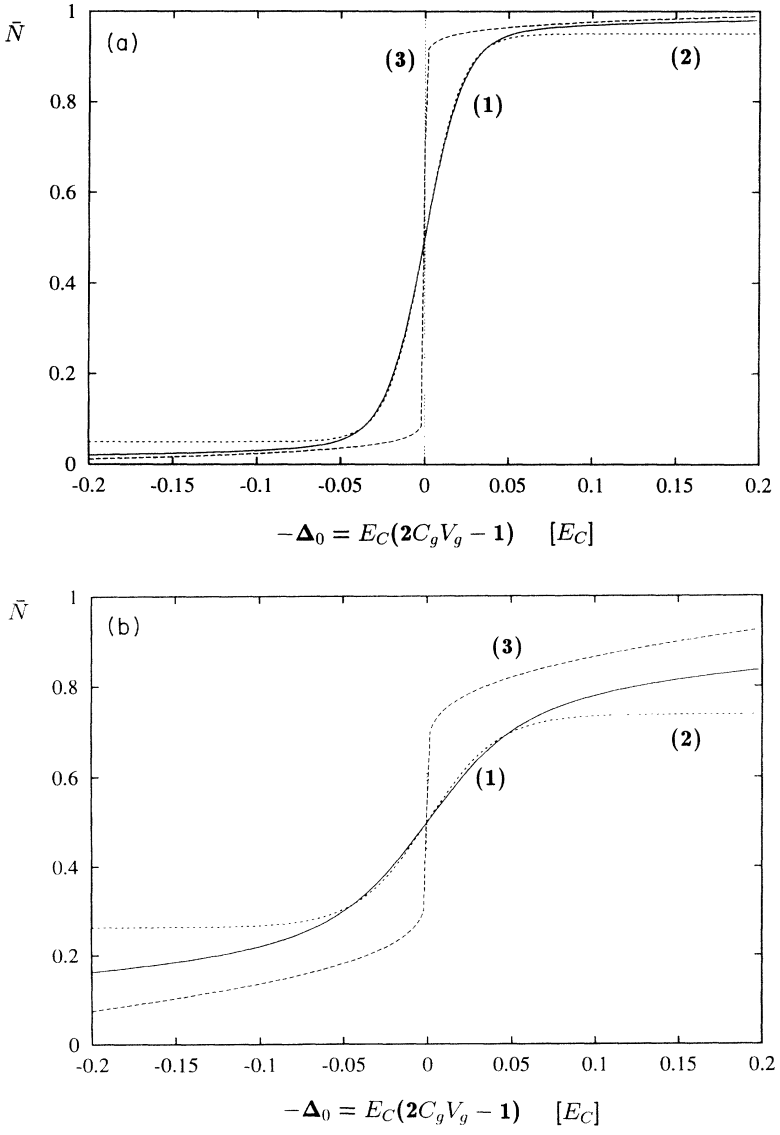

FIG. 21. Average charge as function of the gap energy using (1) the correct result Eq. (67), (2) the fit (71), and (3) the fit (72). $E_C = 1$, $T = 0.01$ and (a) $\alpha_0 = 0.02$ and (b) $\alpha_0 = 0.2$. When finite lifetime broadening effects set on in (b) the deviations grow.

$$\int d\Delta_0\, G(\Delta_0) = \frac{e^2}{h}\pi^4\, \frac{\alpha_0^R \alpha_0^L}{\alpha_0} T. \tag{79}$$

The broadening γ of the conductance peak is then given by

$$\gamma \cong \frac{\int d\Delta_0\, G(\Delta_0)}{G_{\max}} = \frac{\pi^3 T[1 + 2\alpha_0 \ln(\frac{E_C}{2\pi T})]}{\pi - 2\arctan(\frac{(\pi\tilde{\alpha}_0)^2 - 1}{2\tilde{\alpha}_0 \pi})}. \tag{80}$$

In the regime $\pi\tilde{\alpha}_0 \ll 1$, (78) and (80) reduce to

$$G_{\max} \cong \frac{e^2}{h} 2\pi^2\, \frac{\alpha_0^R \alpha_0^L}{\alpha_0} \frac{1}{1 + 2\alpha_0 \ln(\frac{E_C}{2\pi T})} \tag{81}$$

$$\gamma \cong \frac{\pi^2}{2} T \left[1 + 2\alpha_0 \ln\left(\frac{E_C}{2\pi T}\right)\right]. \tag{82}$$

From these results, we can make the following predictions which might be observable in a real experiment. In the regime $2\alpha_0 \ln(\frac{E_C}{2\pi T}) \ll 1$, $G_{\max}$ is constant and γ is proportional to T, which is the classical result from sequential tunneling. For $2\alpha_0 \ln(\frac{E_C}{2\pi T}) \sim 1$ and $\pi\tilde{\alpha}_0 \ll 1$, $G_{\max}$ and γ contain logarithmic terms in the temperature which are an indication for energy renormalization effects due to higher-order tunneling processes. For $T \to 0$, we have

$$G_{\max} \sim \frac{1}{\ln T}, \qquad \gamma \sim T \ln T, \tag{83}$$

i.e., the maximum value as well as the broadening go to zero. For $2\alpha_0 \ln(\frac{E_C}{2\pi T}) \sim 1$ and $\pi\tilde{\alpha}_0 \sim 1$, we have to account for energy renormalization effects as well as effects from finite lifetimes which lead to the complex formulas (78) and (80). Figure 22 shows the conductance versus Δ_0 for several temperatures calculated numerically from the correct formula (76) which demonstrates the predicted behavior.

With respect to the conductance apart from the degeneracy point $\Delta_0 = 0$, we can make the following analytic analysis. For $\tilde{\Delta}_0 \le T$ and $\pi\tilde{\alpha}_0 \ll 1$, we can replace the last fraction in Eq. (77) by $\delta(\omega - \tilde{\Delta}_0)$ since the broadening is of the order $\pi\tilde{\alpha}_0 T \ll T$ and the function $\frac{\omega/T}{\sinh(\omega/T)}$ is varying on a scale of $\omega \sim T$. Thus, we obtain

$$G = \frac{e^2}{h} 2\pi^2\, \frac{\tilde{\alpha}_0^R \tilde{\alpha}_0^L}{\tilde{\alpha}_0} \frac{\tilde{\Delta}_0/T}{\sinh(\tilde{\Delta}_0/T)}, \quad \tilde{\Delta}_0 \le T, \quad \pi\tilde{\alpha}_0 \ll 1, \tag{84}$$

which is the classical result but with renormalized parameters $\tilde{\Delta}_0$ and $\tilde{\alpha}_0$.

For $\tilde{\Delta}_0 \gg T$ and $\pi\tilde{\alpha}_0 \le 1$, we can replace the last denominator in Eq. (77) by $\frac{1}{\tilde{\Delta}_0^2}$ since $\omega \le T \ll \tilde{\Delta}_0$ and $\pi\tilde{\alpha}_0\omega \le \pi\tilde{\alpha}_0 T \le T \ll \tilde{\Delta}_0$. This gives

$$G = \frac{e^2}{h} \frac{8\pi^4}{3} \alpha_0^R \alpha_0^L \left(\frac{T}{\Delta_0}\right)^2, \quad \tilde{\Delta}_0 \gg T, \quad \pi\tilde{\alpha}_0 \le 1, \tag{85}$$

where the renormalization factor $[1 + 2\alpha_0 \ln(\frac{E_C}{2\pi T})]^{-1}$ has dropped out. Thus, in the Coulomb-blockade regime, we recover the usual expression of inelastic electron cotunneling[16,17] provided that $\pi\tilde{\alpha}_0 \le 1$ and $\tilde{\Delta}_0 \gg T$. Therefore, the influence of resonant tunneling processes seems to be easier observable at resonance where $\tilde{\Delta}_0 \le T$. Here, we expect significant deviations from sequential tunneling already in the regime $2\alpha_0 \ln(\frac{E_C}{2\pi T}) \sim 1$ and effects from finite lifetimes [see Eq. (78)] for $\pi\tilde{\alpha}_0 \sim 1$.

Finally, we will compare our result (77) with the one obtained in Ref. 20 which also coincides with other approaches.[18,19,21,22] It reads

$$G = \frac{e^2}{h} 2\pi^2\, \frac{\alpha_0^R \alpha_0^L}{\alpha_0} \int d\omega \frac{\omega/T}{\sinh(\omega/T)} \times \frac{\alpha_0\, \omega \coth(\frac{\omega}{2T})}{(\omega - \Delta_0)^2 + [\pi\alpha_0 \Delta_0 \coth(\frac{\Delta_0}{2T})]^2}. \tag{86}$$

Here, the energy renormalization effects in α_0 and Δ_0 have been neglected and the integration variable ω is replaced by Δ_0 in the broadening part of the last denominator. This corresponds to the introduction of a constant

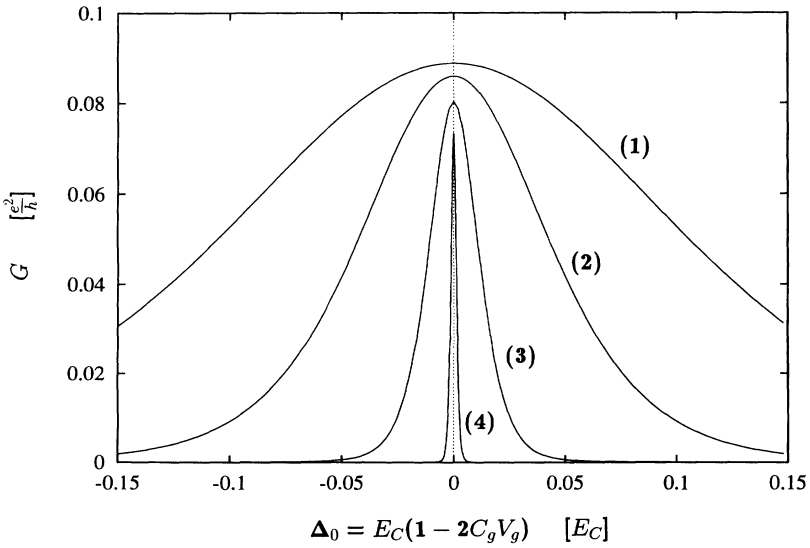

FIG. 22. Conductance as function of the gap energy for various temperatures. $E_C = 1$, $\alpha_0 = 0.02$ and (1) $T = 0.05$, (2) $T = 0.02$, (3) $T = 0.005$, and (4) $T = 0.0005$.

and finite lifetime into the usual expressions of inelastic electron cotunnneling[16,17] which regularizes the integrals. This is only justified in the regime $2\alpha_0 \ln(\frac{E_C}{2\pi T}) \ll 1$, where the renormalization factor $[1+2\alpha_0 \ln(\frac{E_C}{2\pi T})]^{-1}$ and the broadening $\pi\tilde{\alpha}_0\omega \coth(\frac{\omega}{2T}) \sim \pi\alpha_0 T \ll T$ are unimportant. Thus, the replacement $\omega \to \Delta_0$ within the broadening does not change the result for sequential tunneling significantly ($\Delta_0 \leq T$) and for $\Delta_0 \gg T$ Eq. (86) leads to the correct value for electron cotunneling since the numerator of the last fraction of Eq. (77) has not been changed. However, for $2\alpha_0 \ln(\frac{E_C}{2\pi T}) \sim 1$ or $\pi\tilde{\alpha}_0 \sim 1$, Eq. (86) can no longer be used at resonance as is demonstrated in Fig. 23.

VI. CONCLUSIONS

In this paper, we have aimed at presenting a detailed theory of quantum fluctuation effects in transport through small metallic islands with strong Coulomb interaction. With the help of a diagrammatic technique in real-time space, we have identified and evaluated the contribution of correlated higher-order tunneling events. Assuming a wide junction with many transverse channels, we have allowed different electrons to tunnel an arbitrary number of times coherently between the leads and the metallic island. Using the two charge state approximation, we have included in a closed analytic form sequential tunneling, inelastic electron cotunneling, and resonant tunneling processes.

From a theoretical point of view it has turned out that the effects of quantum fluctuations can be understood very clearly by investigating the spectral density which describes the charge excitations of the system. In the classical regime, the spectral density has a sharp maximum at the gap energy Δ_0 which is the difference of the Coulomb energies of two adjacent charge states. In the quantum regime, the maximum point renormalizes to $\tilde{\Delta}_0$ and we obtain a finite broadening which can be esti-

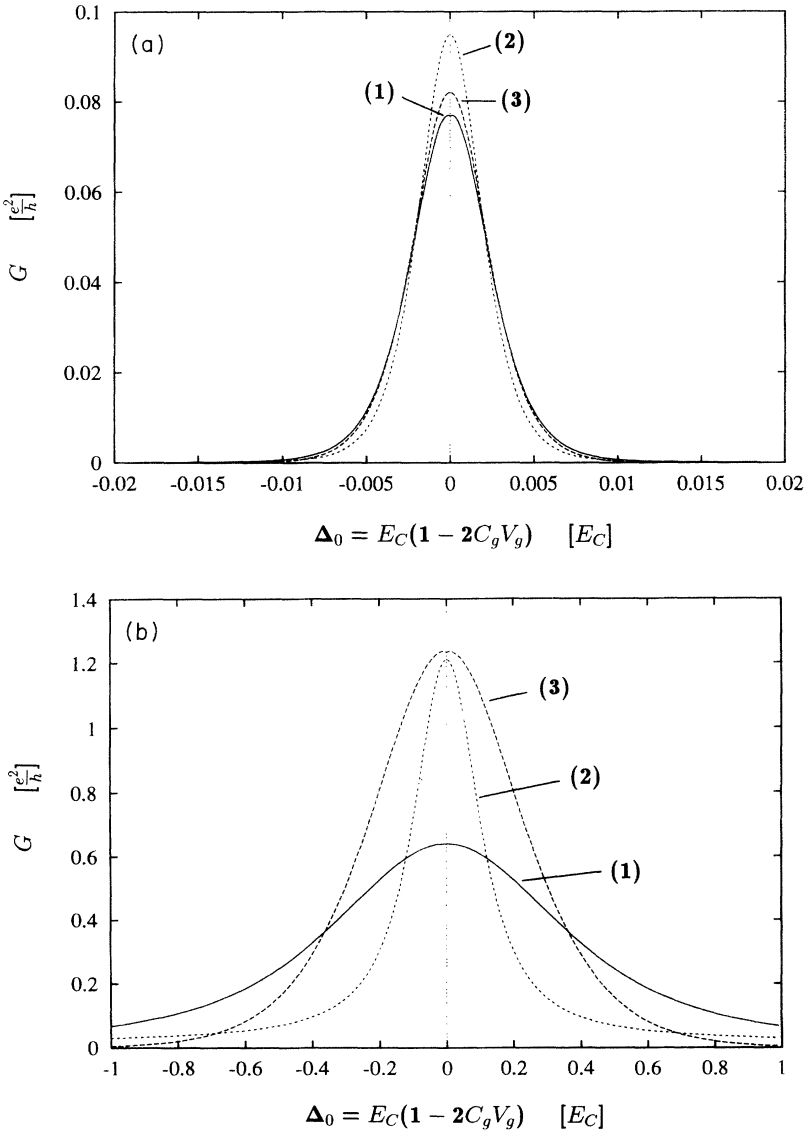

FIG. 23. Conductance as function of the gap energy using (1) the correct result (76), (2) the fit (86), and (3) the fit (84). $E_C = 1$ and (a) $T = 0.001$, $\alpha_0 = 0.02$, and (b) $T = 0.05$, $\alpha_0 = 0.6$. In both cases are clear differences to the classical result (86). (a) can be described by renormalized parameters given by (84), whereas in (b) finite lifetime broadening effects dominate.

mated to be of the order of $\pi\tilde{\alpha}_0 \max\{\tilde{\Delta}_0, T\}$, where $\tilde{\alpha}_0$ is the renormalized dimensionless conductance of a single barrier. Both features together with the complete form of the spectral density is described by the real and imaginary part of the self-energy $\sigma(\omega)$. It contains an anomalous dependence on energy and temperature which leads to a variety of unexpected features in the line shapes of several experimental quantities.

To estimate the experimental consequences of quantum fluctuations, we have calculated the average charge of the single-electron box and the linear conductance of the SET transistor as function of the gap energy Δ_0 or equivalently the external gate voltage. For the average charge, we have compared our results to previous investigations[11,14] where renormalization group techniques have been used to study the zero temperature case. Using the temperature as a cutoff, one can calculate the average charge from these theories in the two limiting cases $\tilde{\Delta}_0 \gg T$ or $\tilde{\Delta}_0 \leq T$. These results agree with our solution in the case $\pi\tilde{\alpha}_0 \ll 1$, i.e., in the regime where finite lifetime effects are not important. For $\pi\tilde{\alpha}_0 \sim 1$ there are significant deviations at least for $\tilde{\Delta}_0 \geq T$. Furthermore, our complete solution is capable of describing the complete crossover from $\tilde{\Delta}_0 \leq T$ to $\tilde{\Delta}_0 \gg T$ and shows that the temperature has to be introduced into the renormalization of the system parameters by the replacement $\tilde{\Delta}_0 \to 2\pi T$.

For the conductance in the linear response regime we have seen that the classical description of sequential tunneling near the resonance ($\tilde{\Delta}_0 \leq T$) is only valid for $2\alpha_0 \ln(\frac{E_C}{2\pi T}) \ll 1$ and $\pi\tilde{\alpha}_0 = \pi\alpha_0/[1 + 2\alpha_0 \ln(\frac{E_C}{2\pi T})] \ll 1$. Nowadays, it is possible to leave this regime experimentally. Therefore, we expect that resonant tunneling of coherent higher-order tunneling processes should be observable in a real experiment by measuring the line shape of the conductance peaks as function of α_0 and temperature. The renormalization of the system parameters Δ_0 and α_0 is important for $2\alpha_0 \ln(\frac{E_C}{2\pi T}) \sim 1$ and leads to an anomalous logarithmic temperature dependence of the conductance peak and the broadening. For $T \to 0$ the conductance maximum goes down to zero like $1/\ln T$ and the broadening increases proportional to $T \ln T$. Furthermore, for $\pi\tilde{\alpha}_0 \sim 1$, the influence of finite lifetimes becomes very important and leads to a very significant flattening of the Coulomb oscillations. Both effects are important and we have seen that it is very difficult to separate them at realistic temperatures.

Finally, our approach describes also correctly the conductance in the Coulomb-blockade regime where transport is dominated by inelastic electron cotunneling. Our analytic formulas give the correct crossover from resonant tunneling at the degeneracy point to inelastic cotunneling. We have seen that cotunneling persists in the regime $\tilde{\Delta}_0 \gg T$ and $\pi\tilde{\alpha}_0 \leq 1$. For $\pi\tilde{\alpha}_0 \gg 1$, cotunneling as well as the validity of our approach will break down. In this regime, the charge will no longer be well defined and one should go beyond the two charge state approximation.

ACKNOWLEDGMENTS

We would like to acknowledge many stimulating and helpful discussions with S.E. Barnes, D. Esteve, H. Grabert, P. Falci, K.A. Matveev, Y.V. Nazarov, A. Schmid, P. Wölfle, A.D. Zaikin, and G. Zimanyi. This work was supported by the Swiss National Science Foundation (H.S.) and by the "Deutsche Forschungsgemeinschaft" as part of "Sonderforschungsbereich 195."

* Present address: Dept. of Physics, Simon Fraser University, Burnaby, B.C., Canada V5A 156.

[1] D.V. Averin and K.K. Likharev, in *Mesoscopic Phenomena in Solids*, edited by B.L. Altshuler, P.A. Lee, and R.A. Webb (Elsevier, Amsterdam, 1991), p. 173.

[2] H. Grabert and M.H. Devoret, in *Single Charge Tunneling*, Vol. 294 of *NATO Advanced Study Institute, Series B: Physics*, edited by H. Grabert and M. H. Devoret (Plenum Press, New York, 1992).

[3] Z. Phys. B **85**, 317 (1991), special issue on single charge tunneling.

[4] I.O. Kulik and R.I. Schekhter, Zh. Eksp. Teor. Fiz. **68**, 623 (1975) [Sov. Phys. JETP **41**, 308 (1975)].

[5] G. Schön and A.D. Zaikin, Phys. Rep. **198**, 237 (1990).

[6] C.W.J. Beenakker, Phys. Rev. B **44**, 1646 (1991).

[7] D.V. Averin, A.N. Korotkov, and K.K. Likharev, Phys. Rev. B **44**, 6199 (1991).

[8] Y. Meir, N.S. Wingreen, and P.A. Lee, Phys. Rev. Lett. **66**, 3048 (1991).

[9] P. Lafarge, H. Pothier, E.R. Williams, D. Esteve, C. Urbina, and M.H. Devoret, Z. Phys. B **85**, 327 (1991).

[10] L.I. Glazman and K.A. Matveev, Zh. Eksp. Teor. Fiz. **98**, 1834 (1990) [Sov. Phys. JETP **71**, 1031 (1990)].

[11] K.A. Matveev, Zh. Eksp. Teor. Fiz. **99**, 1598 (1991) [Sov. Phys. JETP **72**, 892 (1991)].

[12] D.S. Golubev and A.D. Zaikin (unpublished).

[13] H. Grabert, Physica B **194-196**, 1011 (1994).

[14] G. Falci, G. Schön, and G.T. Zimanyi, Physica B (to be published).

[15] W. Zwerger (unpublished).

[16] D.V. Averin and A.A. Odintsov, Phys. Lett. A **140**, 251 (1989).

[17] D.V. Averin and Y.V. Nazarov, Phys. Rev. Lett. **65**, 2446 (1990); in *Single Charge Tunneling* (Ref. 2).

[18] A.N. Korotkov, D.V. Averin, K.K. Likharev, and S.A. Vasenko, in *Single-Electron Tunneling and Mesoscopic Devices*, edited by H. Koch and H. Lübig (Springer, Berlin, 1992).

[19] Y.V. Nazarov, J. Low Temp. Phys. **90**, 77 (1993).

[20] D.V. Averin, Physica **194-196**, 979 (1994).

[21] P. Lafarge and D. Esteve, Phys. Rev. B **48**, 14 309 (1993).

[22] C. Pasquier, U. Meirav, F.I.B. Williams, and D.C. Glattli, Phys. Rev. Lett. **70**, 69 (1993).

[23] L.J. Geerligs, M. Matters, and J.E. Mooij, Physica **194-196**, 1267 (1994).

[24] R.P. Feynman and F.L. Vernon, Ann. Phys. (N.Y.) **24**, 118 (1963).

[25] U. Weiss, *Quantum Dissipative Systems, Series in Modern Condensed Matter Physics* (World Scientific, Singapore, 1993), Vol. 2.

[26] U. Eckern, G. Schön, and V. Ambegaokar, Phys. Rev. B **30**, 6419 (1984).
[27] A.L. Fetter and J.D. Walecka, *Quantum Theory of Many Particle Systems* (McGraw-Hill, New York, 1971).
[28] A.A. Abrikosov, L.P. Gor'kov, and I.Ye. Dzyaloshinskii, *Quantum Field Theoretical Methods in Statistical Physics* (Pergamon Press, Oxford, 1965).
[29] J. Rammer and H. Smith, Rev. Mod. Phys. **58**, 323 (1986).
[30] G.D. Mahan, *Many-Particle Physics*, 2nd ed. (Plenum Press, New York, 1990).
[31] N.E. Bickers, Rev. Mod. Phys. **59**, 845 (1987).
[32] A.C. Hewson, *The Kondo Problem to Heavy Fermions* (Cambridge University Press, Cambridge, England, 1993).
[33] S.E. Barnes, J. Phys. F **7**, 2637 (1977); Phys. Rev. B **33**, 3209 (1986).
[34] J. Rammer, Rev. Mod. Phys. **63**, 781 (1991).
[35] D. Loss and H. Schoeller, Physica A **150**, 199 (1988); J. Stat. Phys. **54**, 765 (1989); **56**, 175 (1989).
[36] H. Schoeller (unpublished).
[37] U. Geigenmüller and G. Schön, Physica B **152**, 186 (1988).
[38] D. Esteve (private communication).